Materials & Design 240 (2024) 112859

Contents lists available at ScienceDirect

Materials & Design

journal homepage: www.elsevier.com/locate/matdes

Multi-stable metastructure with multi-layer and multi-degree of freedom: A numerical and experimental investigation

Shuangfeng Tan [a], Diankun Pan [a,*], Zhangming Wu [a,b]

[a] Key Laboratory of Impact and Safety Engineering, Ministry Education of China, Ningbo University, Ningbo 315211, China
[b] School of Engineering, Cardiff University, Cardiff CF24 3AA, Wales, United Kingdom

ARTICLE INFO

Keywords:
Multi-stable
Metastructure
Multi-layer
Preshaped Beam

ABSTRACT

This paper proposes a family of multi-stable metastructures with multiple layers, which possess the capability of multi-degree of freedom deformations. In its single layer, four preshaped beams connecting two frames are employed as the main component for the design of multi-stable metastructures. Compared with the traditional flat state obtained by axial compression when all beams snap through, four inclined stable states are easy to trigger by lateral compression at a local position when two adjacent beams snap through. The transitions between these states are studied by both experiments and numerical simulation. The transition to inclined states requires less energy than the transition to the flat state. Different trends of load–displacement responses are associated with loading positions and transitions. A parametric analysis is performed to illustrate the relationship between the stability of inclined states and critical parameters, such as span, apex height, and thickness. Two types of hourglass double-layer units are designed and studied through experiments. The continuous transitions in two steps or three steps are observed, and the load–displacement response is the accumulation of responses from each single layer. At last, two multi-layer structures with multi-stability have been developed to demonstrate their deformation capability in multiple directions through multiple steps.

1. Introduction

Mechanical metamaterials or metastructures exhibit unusual properties and functionalities that cannot be realized in conventional materials, such as negative stiffness, negative Posisson's ratio, and negative thermal expansion [1–4]. As an important branch of mechanical metamaterials, negative stiffness metamaterials show promising potential for application in energy absorption [5–7], vibration control [8,9], deployable structure [10,11], energy harvesting [12–14], and soft robotics [15,16].

The negative stiffness of the metamaterials or metastructures arises from the arrangement and construction of certain unit cells, which could be curved beams [17–19], origamis [20–22], composite laminates [23,24] or compliant units [25–27]. The initial curved, double-clamped beam exhibiting elastic instability is one of the most typical unit cells, which is used to construct negative stiffness metamaterials or metastructures. According to the characteristics of the load–displacement curves, the curved beam can be generally classified into two categories: bi-stable and mono-stable. The bistable curved beam exhibiting snap-through behavior can maintain its deformed shape, which corresponds to a local minimum elastic energy value, without requiring external input energy. The monostable curved beam can self-recover to its original shape once the external load is removed.

The curved beam generally has a sinusoidal or cosine shape, and a lot of work has been done to obtain the criteria of bistability [28–30]. By stacking bistable curved beams, the constructed metamaterials or metastructures exhibit multiple stability, which often enables a reversible switching motion. Ren *et al.* [6] proposed a concept of buckling-based negative stiffness lattice materials by adding prefabricated curved beams into bidirectional or tridirectional rigid frames, which are able to undergo multiaxial stress conditions. Hua *et al.* [7,31] investigated the energy absorption ability of the multi-stable planar or cylindrical metastructure consisting of multiple unit cells formed by curved beams in either planar or spatial configurations. Yang and Ma [32] investigated the mechanical behaviors of two kinds of two-dimensional multi-stable mechanical metamaterials, which consist of opposite or parallel curved beams exhibiting elastic snap-through instability mechanisms. Tao *et al.* [11] introduced the shape memory polymer in the construction of multi-stable metamaterials, which can self-expand by heating. Chen *et al.* [33] presented a novel multifunctional negative stiffness meta-structure with

* Corresponding author.
E-mail address: pandiankun@nbu.edu.cn (D. Pan).

https://doi.org/10.1016/j.matdes.2024.112859
Received 5 January 2024; Received in revised form 7 March 2024; Accepted 17 March 2024
Available online 18 March 2024

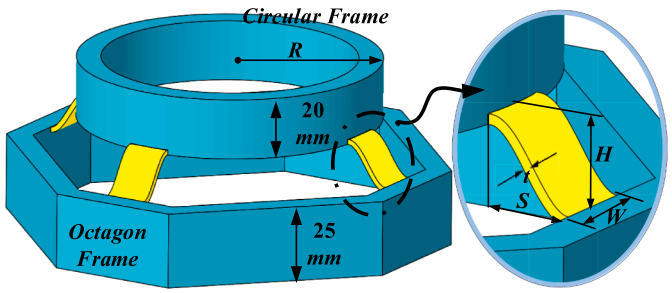

Geometry of beam

Parameters	Value (mm)
R	45
H	11
S	16
W	12
t	1.5

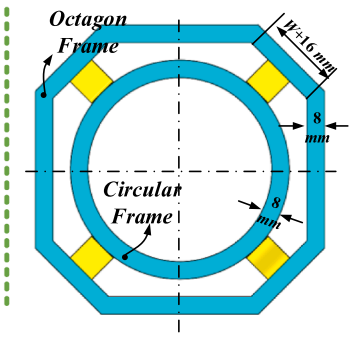

(a) (b)

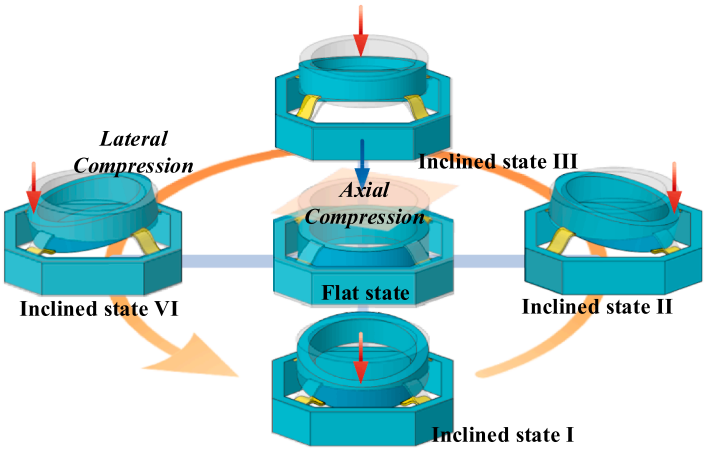

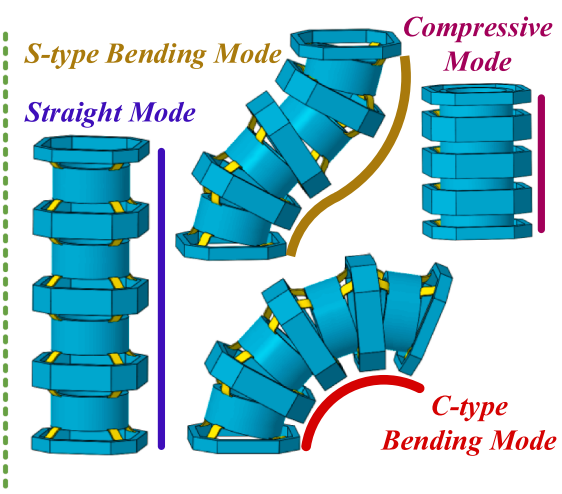

(c) (d)

Fig. 1. (a) The geometry of a single layer; (b) The top view of the single layer; (c) The five stable states of the single layer; (d) The multi-stable metastructure composed of multiple layers.

three layers that can achieve muli-stable or compressive mono-stable properties for a single specimen at the same time. Giri and Mailen [34] manipulated the snapping sequence of bistable lattices incorporated into cylindrical shells by adjusting the thickness of the pre-shaped beams in each layer.

The use of origami units or compliant units provides another important way to construct multi-stability and has been extensively studied. Fang *et al.* [35] investigated the multi-stability characteristics of a stacked origami cellular solid consisting of multiple Miura-ori sheets. Haghpanah *et al.* [36] proposed a family of multi-stable shape-reconfigurable architected materials based on a structural building block encompassing living hinges. Wang *et al.* [37] built a theoretical model to analyze the kinematics and mechanics of the unfolding motion of a square-twist origami. Wickeler et al. [38] proposed a parameterized design for the origami structure composed of interlocking triangles. Furthermore, the bistable laminates are employed as design units to extend the multi-stable design to the field of composite materials. The multi-stable composite structures can be realized using thermally induced composite structures [39–41], pre-stressed composite structures [42,43], and orthotropic composite structures with initial curvature [44,45]. The above multi-stable structures present unique advantages according to their component units and material properties, and have different potential applications, such as the morphing structure exploited by multi-stable composite structures [46–48].

Compared to the multi-stable structures constructed by origami units, compliant units, or bistable laminates, the multi-stable structures composed of curved beams have more simplicity permits, such as rapid application of established for mechanic analysis, performance evaluation, and reliable fabrication. Most previous works of the multi-stable structure constructed by curved beams mainly focused on the quasi-static mechanical properties, especially in the situation of compressive loading. As a result, only the multi-stabilities in the translational motion have been studied. The deformation direction of metamaterials or metastructures depends on the stacking direction of curved beam units, whose deformation leads to planar motion. The deformations of multi-layer metamaterials or metastructures in a planar translational direction can meet the requirements for the applications of energy absorption or vibration control. However, when metamaterials or metastructures are applied for deployable structures or soft robotics, the deformation in a single direction cannot meet the demands for flexible and spatial motions and actions. To enrich the reconfiguration capability of multi-stable structures, Zhang *et al.* [49] investigated the rotational transitions of the multi-stable beam-type metastructures, which consist of two pre-shaped beams in parallel, and the resulting titled stable

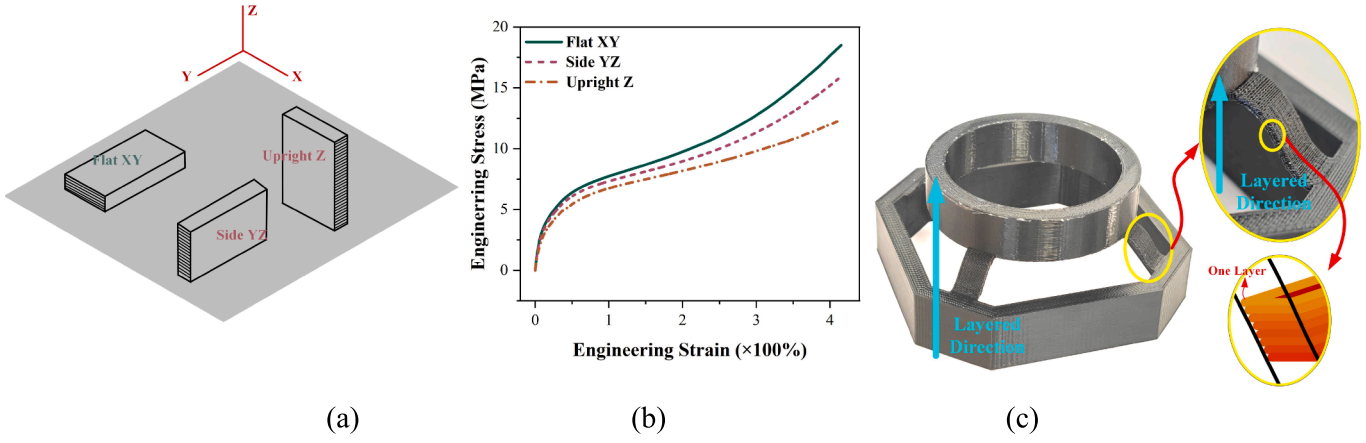

Fig. 2. (a) Three modes during the fused deposition process; (b) Strain-stress curves of TPU; (c) The experimental sample of the single layer.

configurations provide increased degrees of freedom for deformation. Moreover, Zhang *et al.* [50] proposed a family of multi-stable structures composed of prestress unit cells, which have tilted stable configurations and level configurations. Inspired by Zhang's works, we proposed a family of multi-layer, multi-stable metastructures with multiple degrees of freedom in this paper. The pre-shaped curved beams employed to be the deformation elements are distributed spatially and connect two frames to form a single layer that has the capability of bending and stretching. After stacking several single layers of unit cells in the transverse direction, a multi-stable meta-structure, which possesses many postures, is obtained.

In this work, the basic mechanical properties of the proposed single layer when it transits between different stable states are investigated, and then the double-layer unit is proposed to explore the design space. Next, two multi-stable structures with multiple layers are fabricated to demonstrate the deformation ability. The remainder of this paper is organized as follows: Section 2 describes the basic structural design, and Sections 3 and 4 introduce the experiments and numerical method. The results and discussion are listed in Section 5. At last, conclusions are presented in Section 6.

2. Structural design

In this work, the proposed multi-stable metastructure is constructed by multiple layers, and its single layer as the basic design unit determines its mechanical properties. Fig. 1(a) demonstrates the basic components of a single layer. Several pre-shaped beams acting as the deformation components connect two frames, one with a circular shape and the other with an octagonal shape, respectively. The shape of the beam is described by a cosine function ($y=\pm H/2\cos(\pi x/S)$, $[0, S]$), which is able to achieve a smooth snap-through transition before and after large deformation. The basic geometry parameters of the shape include the apex height H, beam width W, span S, and thickness t, as shown in the enlarged view of Fig. 1(a). These parameters, which have been well chosen to be representative according to the requirements and limitations of manufacturing and testing, are listed in Fig. 1(a). Here, the number of beams is 4, and the beams distribute uniformly between the inner circular frame and the outer octagon frame. The width of the two frames is 8 mm, and the outer radius of the circular frame is R, which is defined as a variable, and the length of the side on the octagon frame for connection with beams is 16 mm wider than that of the beam, as illustrated in Fig. 1(b). The remaining size of the octagon frame is determined by the size of the circular frame and the geometry of the preshaped beams. Two frames with enough stiffness barely deform during the transition of stable states, which provide sufficient support and connection between the layers. To provide enough space for the deformation of beams, the heights of the two frames are 20 mm and 25 mm, respectively.

The bistability of the cosine curved beams has been widely investigated [28,51–53], and the transitions of the initial state to the second stable state, namely, the snap-through process, are often triggered by the axial compression. In this work, the proposed single layer can also be triggered by a compressive load, which is applied through a rigid plane covering the upper surface of the circular frame to obtain its flat stable state, as shown in Fig. 1(c). The translation transition from the initial state to the flat state is accompanied by the beams in the same layer deforming synchronously. However, for this proposed single-layer component, the four pre-shaped beams, which are distributed spatially, offer more deformation possibilities than the conventional planar bistable structures. As shown in Fig. 1(c), the single layer possesses the potential to have four inclined stable states, which are achieved by the different deformation states of four beams, including two downward beams and two upward beams. To trigger the transition from the initial state to the inclined state, a concentrated load is applied to the local position of the circular frame to develop an effect of lateral compression. From the initial state to the inclined state, the inclined angle will form between the circular frame and the octagon frame. As such, a bending mode is obtained, and the bending orientation of the upper circular frame depends on the deformation of the beams.

If many single layers stack along the vertical direction, a family of multi-layer multi-stable metastructures is obtained, as shown in Fig. 1 (d). Its initial state is a straight mode, and the compressive modes are triggered by applying axial compressions. Benefiting from the inclined states of each single layer, this meta-structure has many bending modes, such as C-type bending mode and S-type bending mode, as illustrated in Fig. 1(d). Therefore, this type of metastructure can deform in multiple directions and enable the achievement of many different postures, such as stretching and bending. This work aims to study the mechanical properties of a single layer of this type of metastructure to gain a good understanding of the transition mechanism between different stable states. Then, a double-layer unit is presented to construct the multi-layer structures with deformation capability with muli-degree of freedom.

3. Experiments

3.1. Fabrication

To study the mechanical behaviors of proposed multi-stable metastructures, a series of experimental samples were fabricated via fused deposition modeling (FDM) using flexible thermoplastic polyurethanes (TPU). TPU has large recoverable elastic strains, and its material properties were measured by uniaxial loading tests according to ASTM D3039. As the fused deposition process produces parts in a layered structure, the mechanical properties of the part vary depending on its

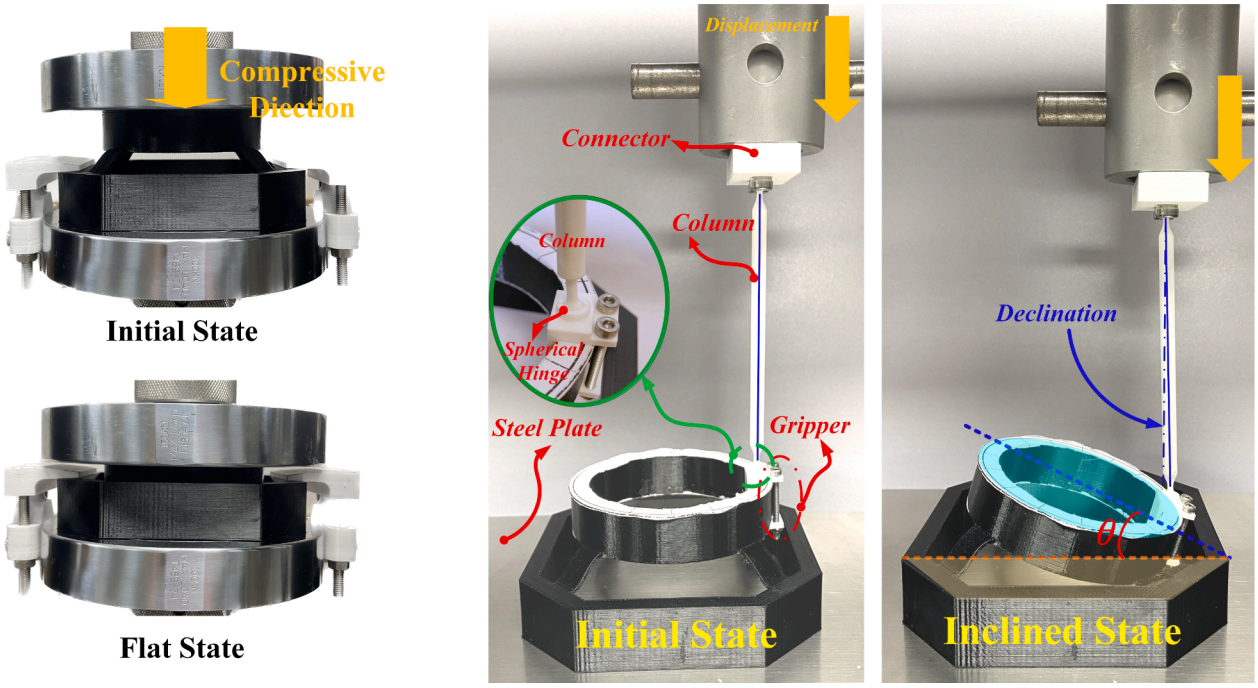

Fig. 3. (a) Two states of axial compression; (b) Experimental setup for lateral compression.

orientation. The specimens could be printed in three modes, which are Flat XY, Side YZ, and Upright Z, as demonstrated in Fig. 2(a). Here, the specimens of all three modes were fabricated and subjected to tensile tests, and the results of strain–stress curves are listed in Fig. 2(b). The sample of the Upright Z mode has a clear difference from the other two modes. Flat XY mode or Side YZ mode is employed in most works due to its high strength. However, limited by the manufacturing technique, the layered direction during the manufacturing process is along the height of the pre-shaped beams, as shown in Fig. 2(c). Therefore, Upright Z mode is employed for manufacturing experimental samples in this work, and the corresponding strain–stress results are utilized to perform the finite element model later. Moreover, it is observed from the enlarged view that the beam has some unavoidable imperfections induced by this fabrication mode. The height of each printing layer is 0.2 mm, and the preshaped beam is formed by stacking these layers. As a result, the surface of the fabricated beam is not as smooth as the ideal situation but is rough like a ladder, as illustrated in Fig. 2(c). This type of imperfection undoubtedly weakens the stiffness of the beams due to the reduced cross-sectional area. This eventually causes the actual load-bearing capacity of the experimental samples to be lower than that of the ideal situation. Besides these primary imperfection conditions, other factors, such as pores and nonuniformity introduced during the manufacturing process can also reduce the mechanical properties of the beams. Moreover, these imperfections result in mechanical variations among the four beams. However, despite the existence of imperfections, beams were not broken during the whole experiment due to the large elastic deformation ability of TPU.

3.2. Experimental tests

A series of compressive loading tests were conducted to generate the load–displacement curves depicting transitions between different states of a single layer. Displacement-controlled quasi-static loading conditions were applied to the experimental sample by a testing system of Instron 5966 with a loading rate of 5 mm/min. To achieve the transition from the initial state to the flat state, two compression plates are employed, as shown in Fig. 3(a). The experimental sample was secured onto the bottom compression plate using two clamps, and an adhesive layer was applied before the upper compression plate made contact with the sample. In doing so, the slipping can be avoided during the testing process. After the testing, the sample was compressed completely under a sufficiently large vertical displacement, as shown in Fig. 3(a). Five tests were carried out, and then the mean value and standard deviation of five load–displacement curves were obtained as the final results.

For the measurement of the rotational transition from the initial state to the inclined state, the bottom compression plate was kept and covered by a steel plate with a larger area, and the top compression plate was replaced by a loading tool consisting of a gripper, a column, and a connector, which were manufactured by FDM using polylactic acid (PLA), as illustrated in Fig. 3(b). The gripper was used to secure a segment of the inner circular frame at the loading position using bolts. The connector is linked to the compression head, while the column with high stiffness connects the connector and the gripper is used for transferring the load. As the top compression head moved, a compressive load was applied to the local region of the circular frame, causing the sample to transit from its initial state to an inclined state. Simultaneously, the bottom surface of the octagon frame was bonded to the steel plate using an adhesive layer to ensure the stability of the whole structure. Herein, this testing process is termed lateral compression. The loading history was recorded, and both the corresponding vertical displacement and the inclined angle between the upper plane and the lower plane, as shown in Fig. 3(b), were measured and recorded. It is worth noting that the column will tilt during the transition of states so that spherical hinges are assigned to both ends of the column, as illustrated in the enlarged view of Fig. 3(b). Because the length of the column is large enough, the declination angle is relatively small, and its effect on the load–displacement results can be neglected. The measurements for other transitions involving inclined states adopted a similar testing setup.

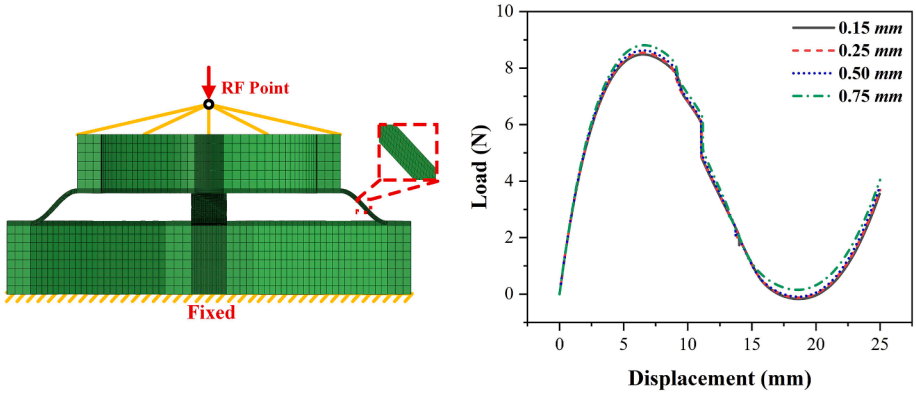

Fig. 4. (a) Numerical model for the axial compression; (b) Load-displacement curves of convergence analysis of finite element model.

4. Numerical simulations

Numerical simulation was employed as the primary analysis method to investigate the mechanical properties of these proposed multi-stable structures. The geometry model of the single layer was established by the software Solidworks and subsequently imported into the finite element method software ABAQUS/Standard. A Marlow hyper-elastic material model utilizing parameters derived from the experimentally measured stress–strain curve of TPU as illustrated in Fig. 2(b), was used for the constitutive relation in finite element analysis (FEA). Throughout the analysis, the 'Nlgeom' (geometrically nonlinear algorithms) setting remained 'ON', and automatic stabilization with a dissipated energy fraction of 2.0×10^{-4} was implemented to ensure computational convergence.

To simulate the behavior of the single layer under axial compression, the bottom surface of the octagon frame was fully fixed, and a reference point was employed by a coupling constraint with the upper surface of the circular frame. It has only one displacement degree of freedom, which is utilized to control the axial compression, as shown in Fig. 4(a). A suitable vertical displacement was applied to the reference point to trigger the transition from the initial state to the flat state in the first 'general, static' step, followed by the acquisition of reaction load–displacement responses during the transition process. Subsequently, another 'static, general' step was carried out to eliminate the displacement and estimate the stability. If the system fails to return to the initial state but stabilizes at a new equilibrium state, it indicates that the current state is stable.

For lateral compression, the bottom surface of the octagon frame remained fully constrained, while a specific vertical displacement was applied to a designated loading point on the top surface of the circular frame to trigger the transition from the initial state to the inclined state in the first 'general, static' step. The position of the loading point, as a variable, will be studied later. Reaction load–displacement curves corresponding to this step were obtained. Subsequently, a second 'general, static' step was required to assess the stability of the inclined state, followed by the measurement of the inclined angle between the circular frame and the octagon frame to characterize the inclined stable state. Additionally, an extra 'static, general' step was appended after arriving at the inclined state, where another vertical displacement was applied to the relevant positions to trigger the transition from the inclined state to another inclined state or a flat state. The load–displacement curves obtained by the above FEA analysis will be discussed and compared with experimental results in the following section.

In this finite element model, eight-node brick elements (C3D8) were used to mesh the structure. The mesh size of the beam with complicated deformation is smaller than that of two frames, which primarily undertake compressive load. Thereby, the computational efficiency was enhanced, and computational time was reduced. For the frames, the mesh size of the remaining parts, except the parts connecting with beams, is 3 mm. A convergence analysis, using lateral compression as an example, was performed, and mesh sizes in the thickness direction of the beams (0.15 mm, 0.25 mm, 0.50 mm, and 0.75 mm) were constructed, as illustrated in Fig. 4(b). As the mesh size of the beam decreases, the load–displacement response stabilizes. Following this convergence analysis and considering computational efficiency, six meshes along the thickness direction were applied.

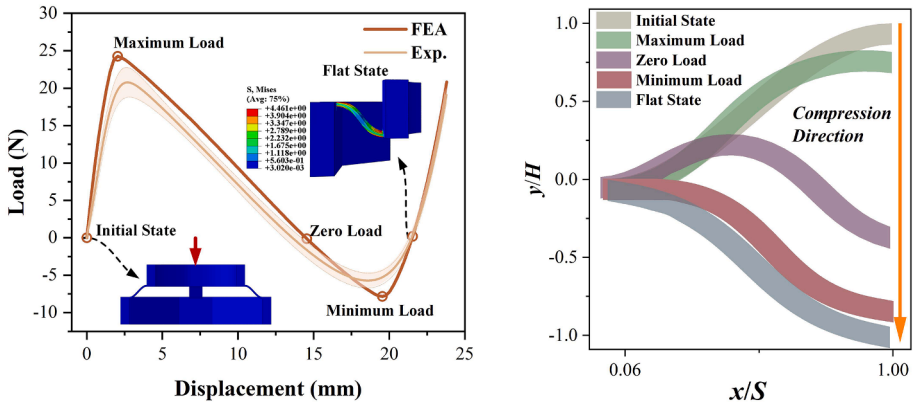

Fig. 5. (a) Load-displacement curves under axial compression; (b) The deformation process of the beam for axial compression predicted by FEA.

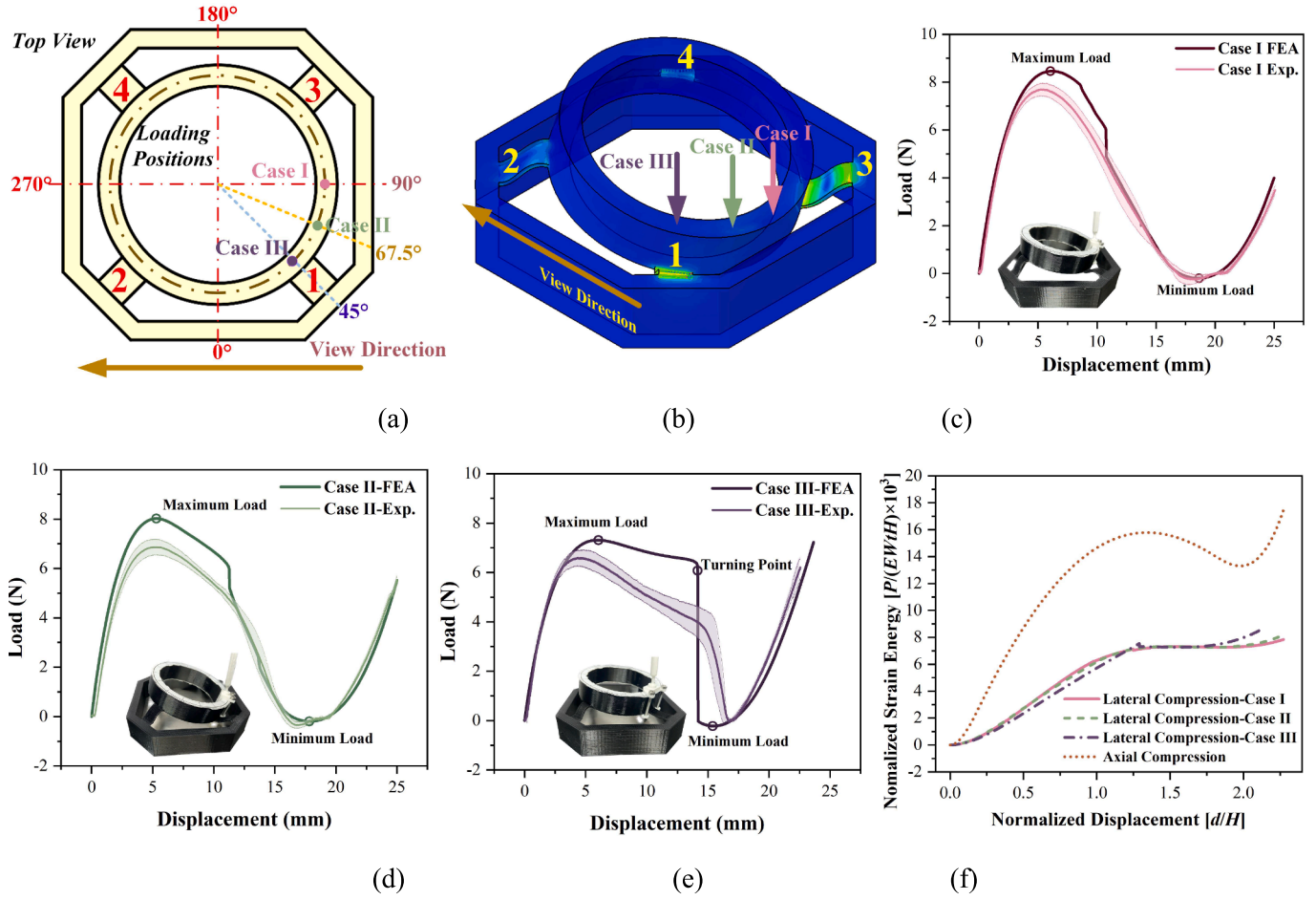

Fig. 6. (a) Three loading positions of lateral compression on the top view of the single layer; (b) The inclined state predicted by FEA; (c) The load–displacement curves of Case I; (d) The load–displacement curves of Case II; (e) The load–displacement curves of Case III; (f) The normalized strain energy with respect to different transitions predicted by FEA.

5. Results and discussion

5.1. Single layer

5.1.1. Axial compression

As a design unit, a single layer of the metastructure proposed in this paper has five stable states after deformation, including one flat state and four inclined states. The transition from the initial state to the flat state under axial compression is the most common. The measured load–displacement curves of axial compression are compared with results predicted by FEA, as shown in Fig. 5(a). It can be observed that there is a good qualitative agreement between experimental and numerical results. However, the maximum load predicted by FEA is higher than the experimental value. It is attributed to the fact that the curved beams become weak due to the imperfections introduced by the manufacturing process. The representative characteristics of bistability, such as the negative stiffness between maximum load and minimum load, and the negative value of minimum load, can be easily identified from the load–displacement curves. Four beams within a single layer of this metastructure have the same deformation at the flat stable state obtained by axial compression, and they mainly exhibit bending modes, as shown in Fig. 5(a). Moreover, the transient shapes of the beam corresponding to the characteristic points in Fig. 5(a) are extracted from FEA results, as shown in Fig. 5(b). It is observed that the beam undergoes bending and compression deformation during the transition from the initial state to the flat state.

5.1.2. Lateral compression

A single layer of the metastructure has four inclined states and one flat state, and its postures can be adjusted by the transitions between different states. In this section, lateral compression is utilized to trigger the state transitions, including initial state to inclined state, inclined state to inclined state, and inclined state to flat state.

1. Initial state to inclined state

Firstly, the inclined state is obtained by lateral compression acting on the circular frame. Due to the circular shape of the upper frame where the load is applied, the angles increasing in an anti-clockwise direction are employed to represent the loading position, as illustrated in Fig. 6(a). To express this easily, the beams are marked with different numbers from 1 to 4, as shown in Fig. 6(a). Three typical loading cases are investigated, respectively. When the load is applied at the middle point of the arc between two beams of No. 1 and No. 3, it is termed Case I, while the loading position is denoted as 90°, as shown in Fig. 6(a) and (b). For Case III, the load acts on the axis of the No. 1 beam, and the loading position is denoted as 45°. The loading position of Case II is located in the middle of Case I and Case III, which is denoted as 67.5°. Due to the central symmetry of the circular frame and the distribution form of beams, the other angles representing the same loading positions exhibit the same mechanical properties in the finite element model. However, the experimental results at the same loading positions with different angles show a certain difference due to the imperfection of the sample. Therefore, four tests were performed for the same position but at different angles, and then the mean value and standard deviation of four load–displacement curves were obtained.

Table 1
The mechanical properties corresponding to different transitions of the single layer.

Transitions		Maximum Load (F_{max})/N		Minimum Load (F_{min})/N	
		Exp. (Mean Value)	FEA	Exp. (Mean Value)	FEA
Initial State to Flat State		20.76	24.25	−5.67	−7.84
Initial State to Inclined State	Case I	7.40	8.46	−0.25	−0.20
	Case II	6.84	8.01	−0.10	−0.19
	Case III	6.08	7.31	−0.01	−0.22
Inclined State to Inclined State		8.01	8.76	−0.72	−0.18
Inclined State to Flat State		10.04	9.73	−1.81	−2.52

For FEA, the same inclined state is obtained under these three loading cases, as shown in Fig. 6(b). In this inclined state, the beams of No. 1 and No. 3 deform downward, and the inclined angle between the two frames predicted by FEA is 15.6°, which is consistent with the average experimental value of 16.1° of the four inclined states. Fig. 6(c) displays the load–displacement curves of Case I, where the load increases to a maximum point first and then decreases to a minimum point. For Case II, the load also increases and then decreases, but a phase with a slow decline appears after the maximum point, as shown in Fig. 6(d). However, the situation becomes different when the load is applied to the beam in Case III. In Fig. 6(e), the load increases to a maximum point and then decreases very slowly to form a platform phase, and an obvious turning point appears before the load falls vertically. The values of maximum load and minimum load in the above three cases are listed in Table 1. The value of maximum load for Case I is the highest among the three loading cases of lateral compression, but there is little difference in the values of minimum load. Furthermore, the value of maximum load in lateral compression is much lower than that of axial compression.

The experimental results generally exhibit basic consistency with the FEA results. However, the experimental maximum loads of three cases are lower than those predicted by FEA, as illustrated in Table 1. This discrepancy is attributed to the imperfections present in the experimental samples, as discussed earlier. The inevitable imperfections of the beam reduce the overall load-bearing capacity of the structure. However, there are noticeable differences in the trend of load–displacement curves between the experimental and FEA results, particularly evident in Case III, as shown in Fig. 6(e). Further analysis will be conducted in the following section to explore the reasons behind these differences, taking into account the deformation process.

The strain energy (P) concerning displacement (d) during the three loading processes is predicted by FEA and then normalized ($E = 56$ MPa) as shown in Fig. 6(f), which is compared to the situation of axial compression. It indicates that the transition from the initial state to the inclined state exhibits a local minimum in the energy landscape, which corresponds to the stable state, but the energy corresponding to the inclined state is much lower than that of the flat stable state. Moreover, the energy well of the inclined state is much shallower than that of the flat state. This illustrates that the inclined state needs less energy to obtain, but the inclined state is not very stable and is easily broken compared to the flat state. Comparing the three cases of lateral compression, Case III needs more energy to reach the inclined state.

The transient shapes corresponding to the characteristic points on the load–displacement curves in Fig. 6 are extracted from the results of FEA, as shown in Fig. 7. To express it concisely and clearly, four beams are retained, and two supporting frames are hidden. The left view is employed as the main view to show the deformation process, and the view direction has been illustrated in Fig. 7. In this view direction, beams No. 1 and No. 2 overlap at the initial state. For Case I, beams No. 1 and No. 3 are symmetric, so they have the same deformation process. Beams No. 1 and No. 3 deform downward with the loading, and beams No. 2 and No. 4 barely change. Different from axial compression, the deformation of the beam unit includes not only bending and compression but also twisting. For Case II, beam No. 1 deforms downward at the point of maximum load, but the deformations of beams No. 1 and No. 3 have synchronized at the point of minimum load. However, the deformation of beams No. 1 and No. 3 become out of sync until the turning point in Case III. During the load-falling process from the turning point to the minimum load, beam No. 3 snaps quickly to follow beam No. 1 and then reaches synchronization at the point of minimum load. Another

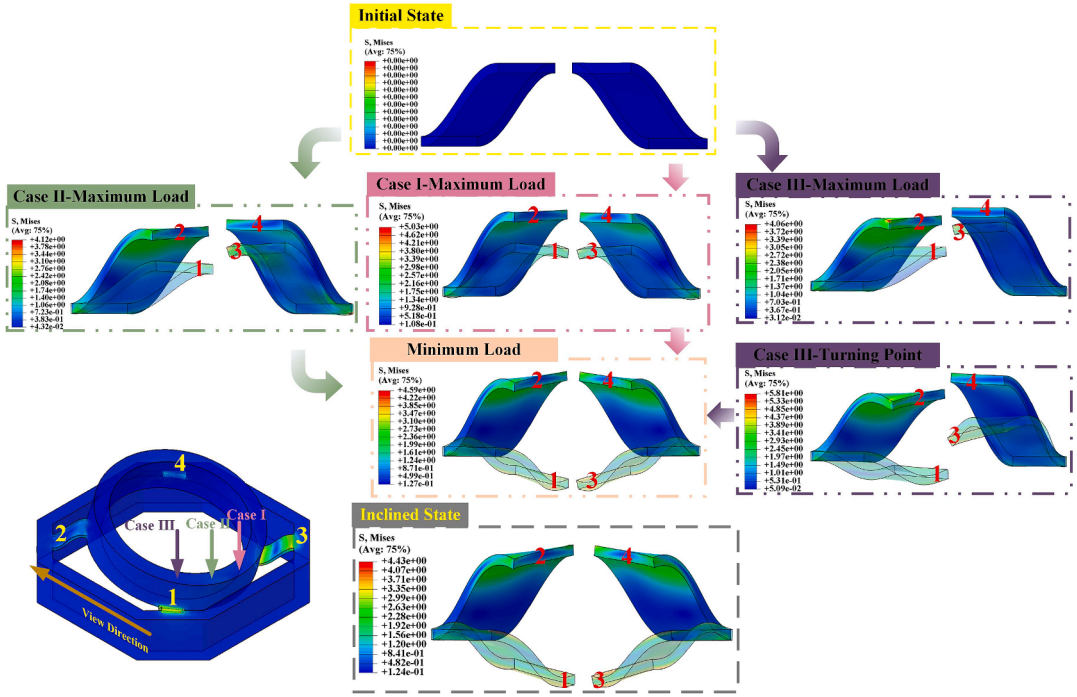

Fig. 7. The deformation process of the beams under different loading cases predicted by FEA.

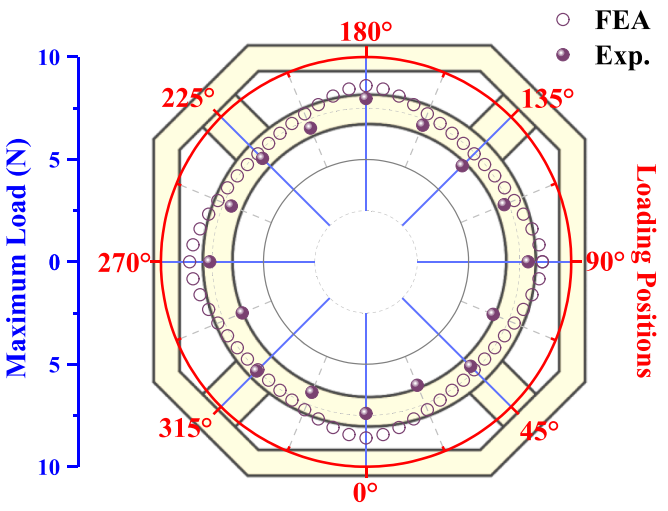

Fig. 8. The maximum load vs loading positions from the initial state to the inclined state.

point that should be noted is that the beam subjected to load exhibits bending and compression without twisting in the platform phase shown in Fig. 6(e).

However, there are observed differences between the experimental deformation processes and the results predicted by FEA, as reflected in the load–displacement curves shown in Fig. 5. In Case III, experiments revealed that beam No. 3 deformed gradually following beam No. 1, resulting in an indistinct platform phase on the experimental load–displacement curve. This discrepancy can be attributed to the fact that the equilibrium state associated with the platform phase is easily disrupted, causing beam No. 3 to start to deform earlier than that predicted by FEA. This early deformation is due to inherent mechanical property variations among the four beams resulting from the imperfection. This discrepancy further contributes to the observed differences between experimental results and FEA results, as illustrated in Fig. 6(e).

The maximum loads with other loading positions are simulated by FEA and compared with experimental results in Fig. 8. When the load is applied to 0°, 90°, 180°, and 270°, the maximum load is the highest. When the load is applied to the beams (45°, 135°, 225°, and 315°), the maximum load is the lowest. When the load is applied to the arc of the circular frame between two beams, the same inclined stable state is obtained. For example, if the load position is located from 45° to 135°, the obtained state will incline in the direction of 90°. When the load is applied to another range of angles, the inclined direction will follow the loading positions such that four inclined directions are enabled by the arrangement of loading positions.

As discussed before, the inclined state is more unstable than the flat state, so it is necessary to find the conditions under which the inclined state loses its stability. However, an accurate theoretical model has yet to be established; a parametric analysis using the finite element model is employed to explore and clarify this issue. As shown in Fig. 9(a), the maximum load (F_{max}) is associated with parameters H and t when H is set to be equal to S and the loading position is similar to Case I. The maximum load is normalized by the elastic parameter E of 56 MPa and the width W of 10 mm. Herein, five different values are assigned to the thickness t of the beam; however, the trends observed across these variations are nearly the same. Therefore, it is believed that the normalized results exhibit universality. The maximum load decreases with the ratio of H and t. When H/t is lower than a certain value, the inclined state is not stable anymore, as marked in Fig. 9(a) with the hollow scatter. Moreover, if H/t is too high, the inclined state will also disappear. Particularly, it is difficult to obtain the inclined stable state when the thickness is relatively high. If a stable inclined state exists, the inclined angle increases with H/t. In Fig. 9(b), the influence of the ratio

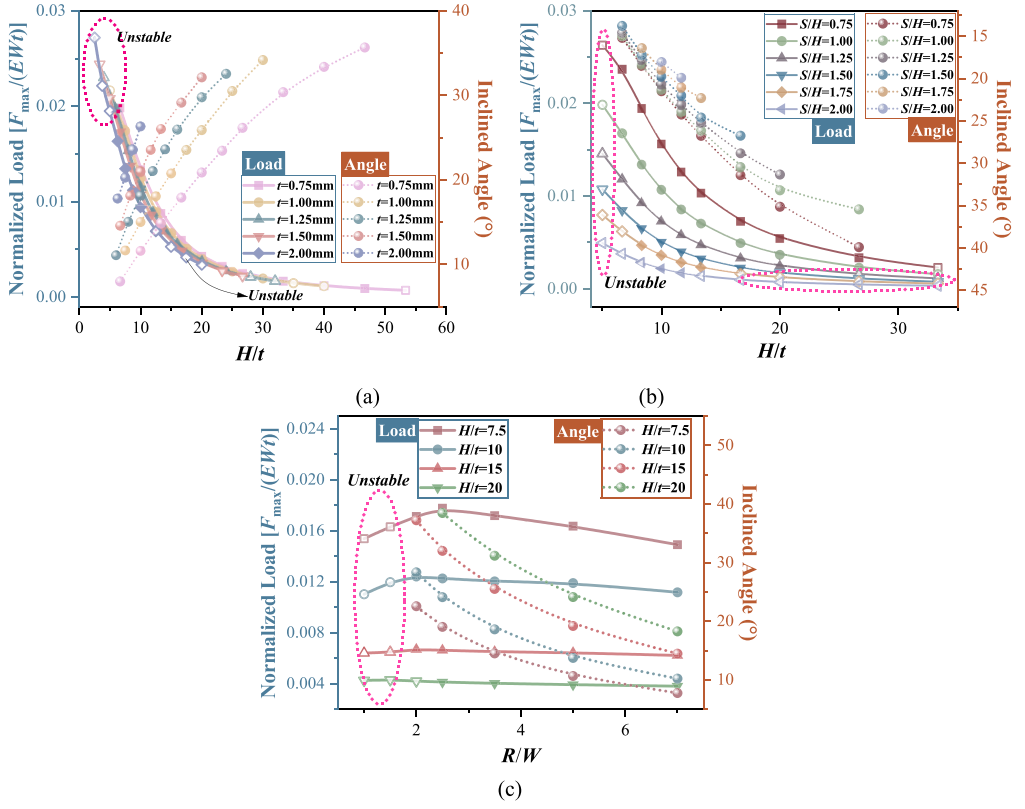

Fig. 9. A parametric analysis predicted by FEA: (a) The maximum load and inclined angle are associated with the parameters of H and t; (b) The maximum load and inclined angle are associated with the parameters of H and S; (c) The maximum load and inclined angle are associated with the parameters of R and H.

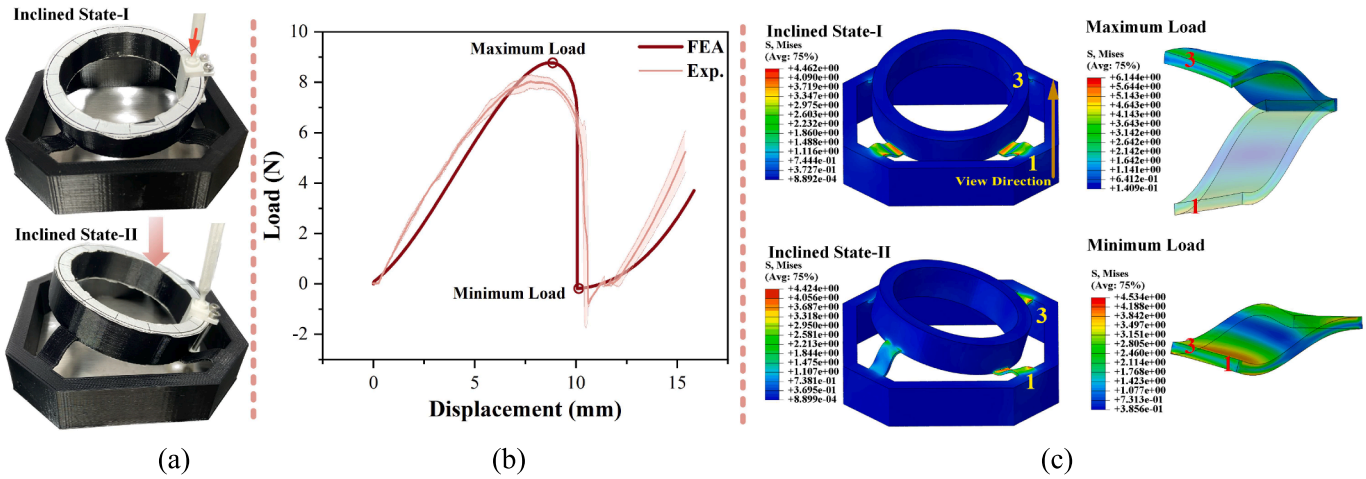

Fig. 10. (a) Two inclined states of experiments; (b) The load–displacement curves corresponding to the transition from the inclined state to the other inclined state; (c) Two inclined states and shapes of beams predicted by FEA.

of S and H is demonstrated. Herein, the thickness t is set to be 1.5 mm, and the width W is 12 mm. It is found that the inclined state is not stable when the ratio of H and t is too high or too low when the ratio of S and H is certain. For a lower ratio of S and H, the inclined stable state will last in a wider range of the ratio of H and t. The inclined angle of the stable state increases with H/t if the inclined stable state exists. If H/t is certain, the inclined angle increases with S/H. Here, to achieve a robust inclined stable state, it is recommended to maintain the H/t ratio within the range of 6.5 to 20, while ensuring the S/H ratio remains below 1.75. Additionally, the influence of the parameter R is shown in Fig. 9(c), while the width W is 10 mm and the thickness t is 1 mm. When R is much higher than W, the load is not affected significantly by R when H/t is certain. However, the inclined angle decreases obviously with R. It is worth noting that stability will disappear when R/W becomes lower. To achieve a stable inclined state, it is recommended to ensure the value of R/W exceeds 2.5. Therefore, the parameters H, S, t, and R could be regarded as the main design variations for determining the existence of the inclined stable state and affecting the mechanical properties. In the design of a single layer, opting for a wider beam (W) rather than increasing its thickness (t) is preferable for enhancing its load-bearing capacity. Because the stability of the inclined state is less influenced by the width (W) compared to the thickness t. If the design objective is based on the inclined angle, tuning the value of S/H is a suitable variable to prioritize.

2. Inclined state to inclined state

There are four inclined states for a single layer of the metastructures, and the transition from one inclined state to another inclined state can be triggered by lateral compression. As shown in Fig. 10(a), one inclined state has been triggered from the initial state by loading at the position of 0° shown in Fig. 6(a), a lateral load continues applying at the position of 90°, and then another inclined state can be obtained. The experimental load–displacement curve is compared to the results of FEA in Fig. 10(b). The load increases slowly to a maximum point, while the stiffness decreases gradually. After the maximum point, the negative stiffness appears briefly, and the load drops to a minimum value, which means a snap-through behavior is triggered. The two inclined states are predicted by FEA, and the corresponding maximum load and minimum load for beams No. 1 and No. 3 are also extracted, as shown in Fig. 10(c). Under the loading, beams No. 1 and No. 3 with different deformation statuses move downward together at first until beam No. 3 snaps, represented by the vertical descent of the load, and the two beams exhibit the same deformation status at the minimum point. The values of the maximum load and minimum load corresponding to this transition are listed in Table 1. Compared to the transition from the initial state to the inclined state, the transition between two adjacent inclined states needs a higher load.

3. Inclined state to flat state

There is a special transition from the inclined state to the flat state, as shown in Fig. 11(a). An inclined state has been obtained by lateral compression at the position of 270° shown in Fig. 6(a), and then a load is applied to the position of 90°, which results in a transition to the flat state. The load–displacement responses corresponding to this transition

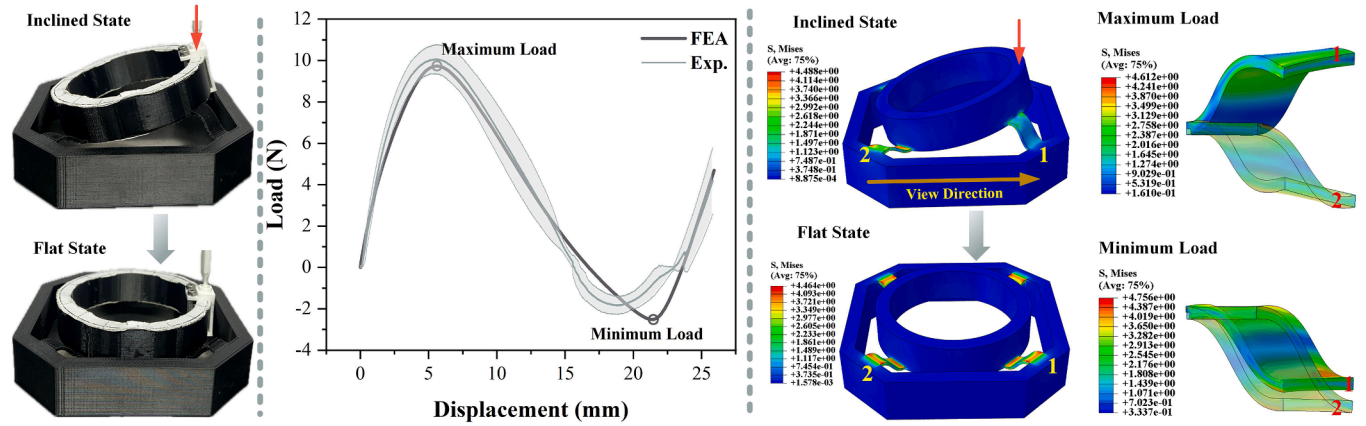

Fig. 11. (a) The inclined state and flat state of experiments; (b) The load–displacement curves corresponding to the transition from the inclined state to the flat state; (c) The inclined state and flat state, and shapes of beams predicted by FEA.

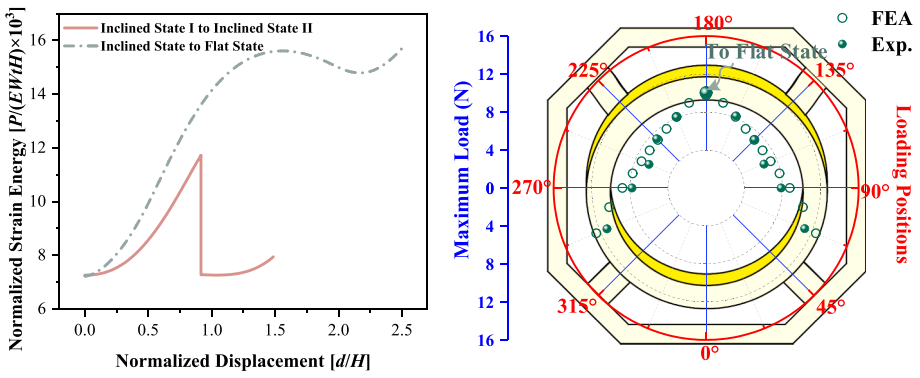

Fig. 12. (a) The strain energy curves of transitions from the inclined state to another inclined state or flat state predicted by FEA; (b) Maximum load vs loading positions from the initial state to the inclined state.

are given in Fig. 11(b). The varying trend of the load–displacement curves is similar to that under axial compression. An obvious stage of negative stiffness arises between the maximum point and the minimum point. However, compared to the axial compression, the value of the maximum load is much lower, as shown in Table 1. As illustrated in Fig. 11(c), beams No. 1 and No. 2 are employed to analyze this transition process. During the early stage of this transition process, beam No. 1 takes the most load and deforms downward, and beam No. 2 barely changes. When the load reaches the lowest value, beam No. 1 completes the transition, shifting from upward to downward.

The curves of strain energy (P) with respect to the displacement corresponding to the two above transitions are predicted by FEA, as shown in Fig. 12(a). The local minimum values of strain energy corresponding to two inclined states are the same, and an energy barrier should be overcome to complete this transition between two inclined stable states. The higher strain energy of the flat state leads to a higher energy barrier, so the corresponding transition is more difficult to finish. Combining the results in Fig. 6(f) and Fig. 12(a), four inclined stable states are located at the same energy levels that are lower than that of the flat stable state. If the imposed external energy is sufficient enough to cross the energy barrier, the transition from the initial state to inclined stable states is easy to trigger, and the flat state is difficult to reach without other constraints. However, the state transitions of the single layer involving snap-through behaviors of beams are nonlinear dynamic processes. When the external energy is sustained input, the transitions from the inclined state to the other inclined state or the flat state may occur. If the external energy is vibration, the cross-well responses between the initial state and inclined states are easy to obtain due to the relatively shallow energy barrier from the inclined state to the initial state. Therefore, understanding the dynamic characteristics of the proposed multi-stable structure is significant, especially when it is used as a morphing mechanism, and should be investigated carefully in the future.

As shown in Fig. 12(b), more loading positions are considered by experiments and FEA. The transition from the inclined state to the flat state is more difficult to trigger, so only the loading position of 180° is available. When the load is applied to the remaining positions, the transitions between adjacent inclined states are completed. However, the transition will not occur if the loading position is too close to the point that triggers the transition from the initial state to the current inclined state. As a result, the angles corresponding to these positions lack load data. The maximum load has the lowest value at the positions of 135° and 225°, which correspond to where two upward beams are.

5.2. *Double-layer unit*

The single layer is not easy to stack directly to construct multi-layer structures due to its cone configuration. Therefore, a construction unit with double layers is designed, as shown in Fig. 13. Two layers are connected by their circular frames to form an hourglass-type unit. If the top layer overlaps with the bottom in the top view, the unit is termed Type I. After rotating the top layer of Type I with an angle of 45°, the beams on the two layers are crisscrossed, and it is named Type II. In this section, these two types of double-layer units are investigated by experiments to exhibit their capability of deformation. The parameters of the single layer remained the same in the above study. In the experiments, the samples with a single layer were fabricated first, and then an adhesive layer of epoxy was employed to bond two single layers to obtain the double-layer samples.

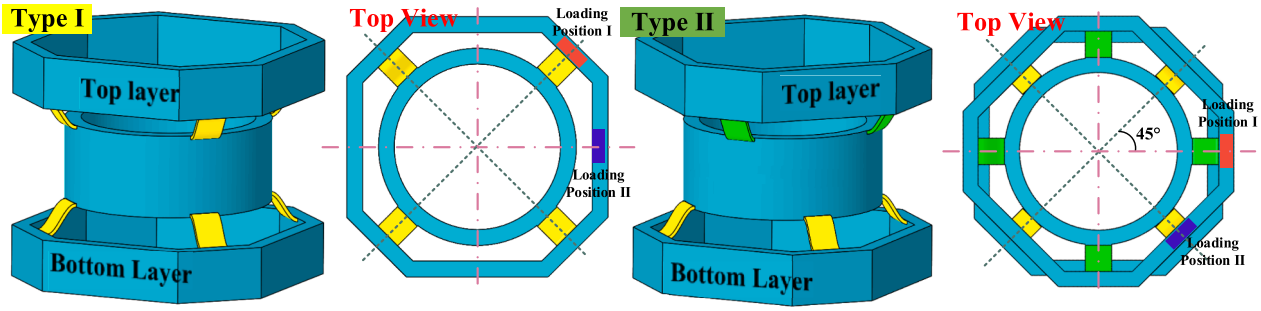

Fig. 13. Two types of double-layer units.

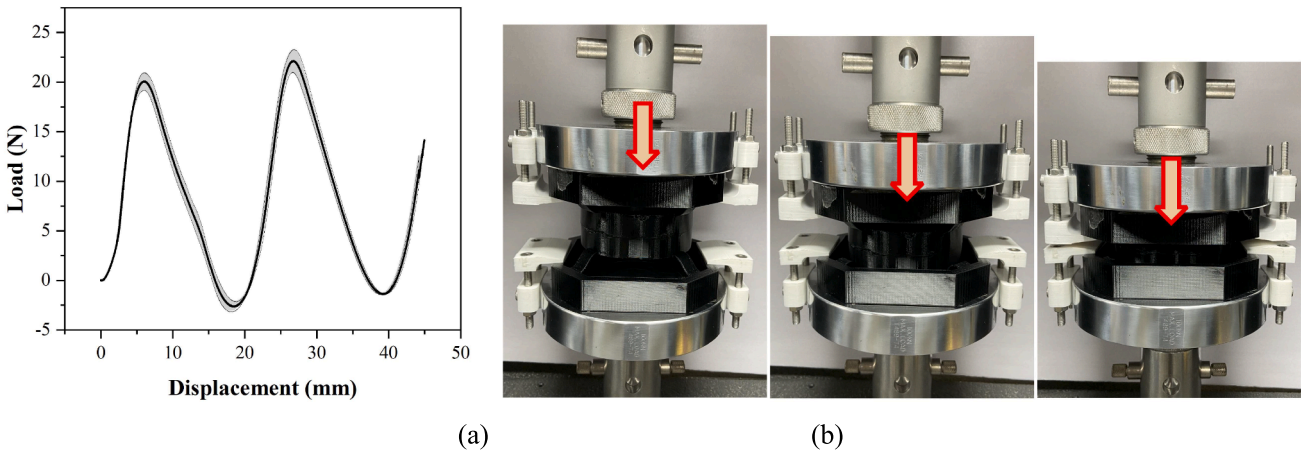

Fig. 14. (a) The experimental load–displacement curves of the double-layer unit from initial state to flat state; (b) The experimental deformation process of the double-layer unit.

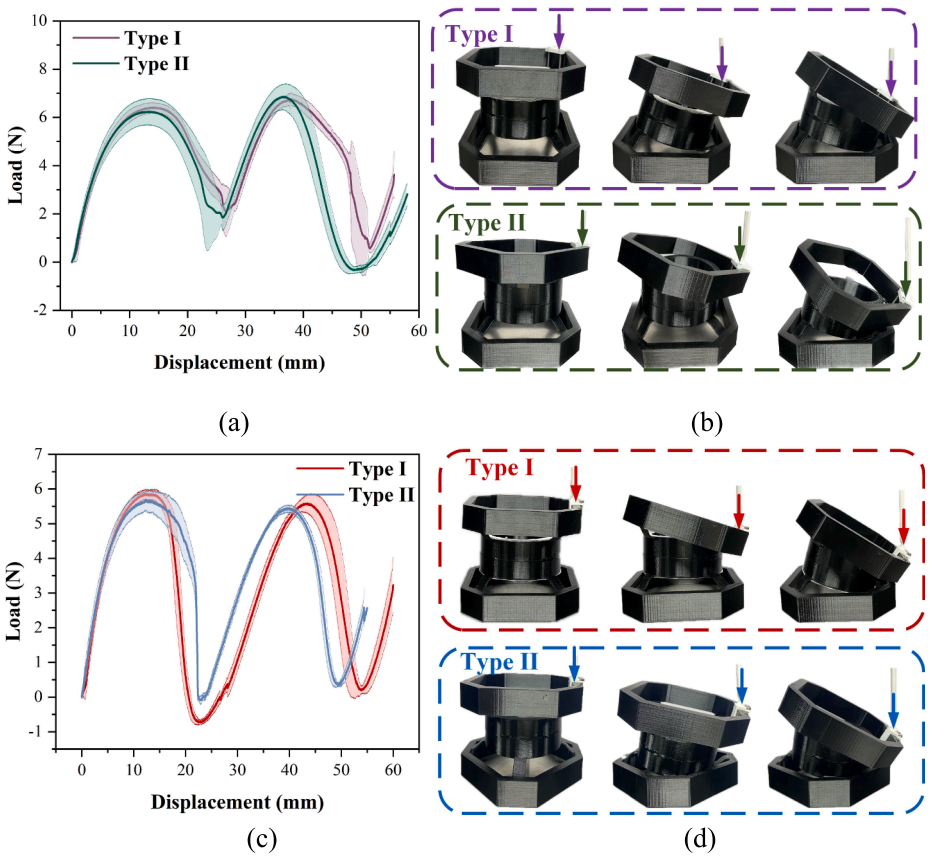

Fig. 15. (a) The experimental load–displacement curves of the double-layer unit from the initial state to the bending state when the load is applied to Position I; (b) The transition order of two types of experimental samples when the load is applied to Position I; (c) The experimental load–displacement curves of the double-layer unit from the initial state to bending state when the load is applied to Position II; (d) The transition order of two types of experimental samples when the load is applied to Position II.

5.2.1. Axial compression

Firstly, the experimental testing for the Type I sample under axial compression was performed, and the experimental load–displacement curves are shown in Fig. 14(a). The load experiences two cycles of increasing and decreasing, which means that each layer exhibits evident snap-through behavior sequentially. As shown in Fig. 14(a), the bottom layer finished the transition first, and then the top layer transitioned from the initial state to the flat state, so the stretching along the height direction could be realized in steps. Two types of double-layer units have the same response under axial compression, so the Type II unit was not studied anymore.

5.2.2. Lateral compression

1. Initial state to bending state

Lateral compression is employed to trigger the transition from the initial state to the bending state of the double-layer unit. Two positions are adopted to investigate the influence of the loading position, as illustrated in Fig. 13. For Position I, the load is applied to the side

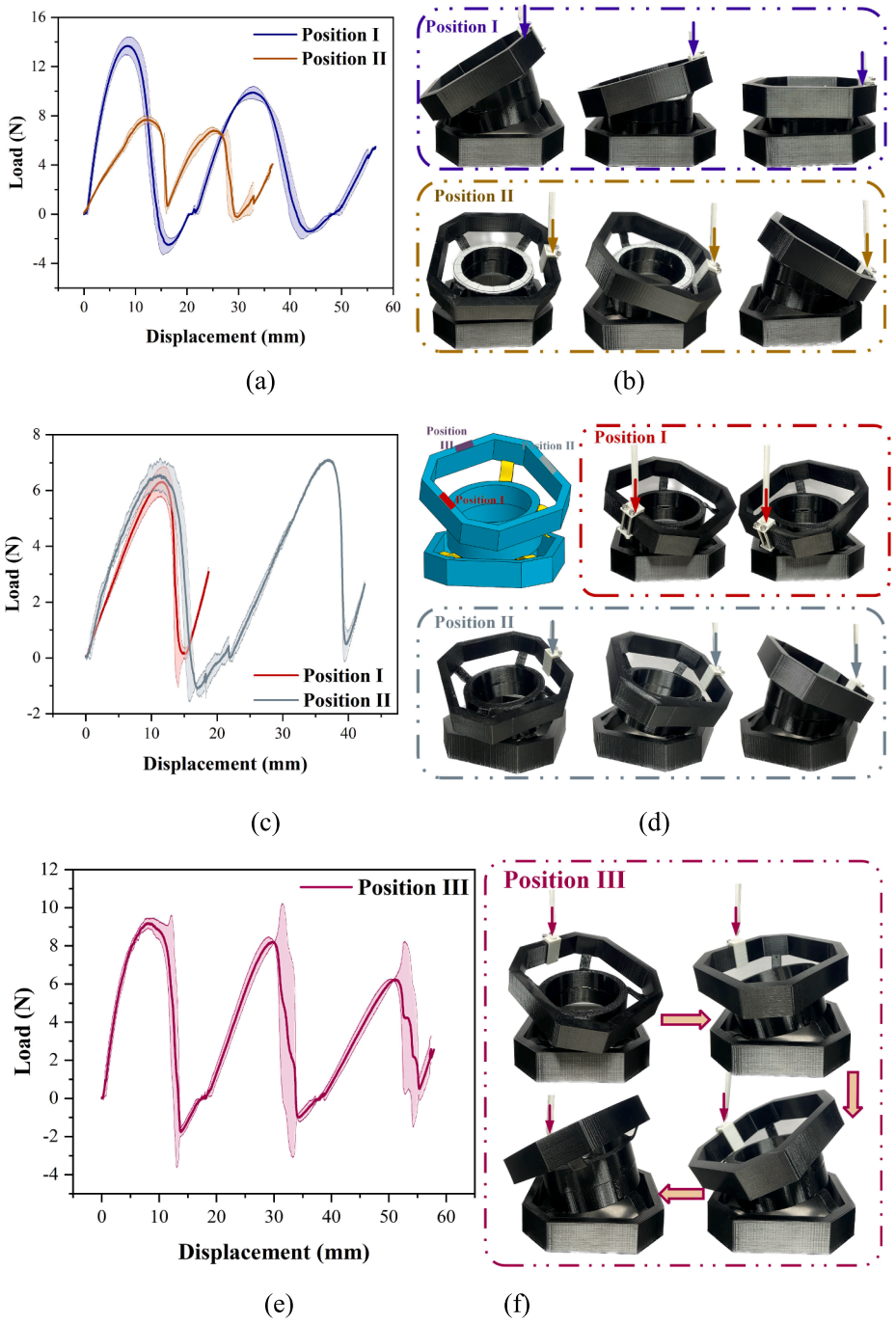

Fig. 16. (a) The experimental load–displacement curves of the double-layer unit (Type I) when the load is applied to Position I and II; (b) The transition orders of experimental samples corresponding to two transitions in (a); (c) The experimental load–displacement curves of the double-layer unit (Type II) when the load is applied to Position I and II; (d) The transition orders of experimental samples corresponding to two transitions in (b); (e) The experimental load–displacement curves of the double-layer unit (Type II) when the load is applied to Position III; (f) The transition order of experimental samples corresponding to the transitions in (e).

connected with the beam of the octagon frame. Fig. 15(a) displays the load–displacement responses of two types of double-layer units when the load is applied to Position I. For Type I, the bottom layer transits to its inclined state in the first step, and a bending state is reached after the transition of the top layer in the second step, as shown in Fig. 15(b). Due to the load applied to the position corresponding to the beam, the varying trend of the load–displacement response for a single transition of two steps is similar to Case III in Fig. 6(e). For Type II, the top layer inclines first, and then the bottom layer transits, as shown in Fig. 15(b). The bending angle of the two layers is not in the same plane, so the different bending orientations could also be realized in the same double-layer unit. Its loading situation is similar to Case III for its top layer and becomes the situation of Case I for the bottom layer, so the trend of load–displacement response is regarded as a superposition of these two transitions. The load is shifted to the position between the beams, and this case is termed Position II, as shown in Fig. 13. Fig. 15(c) shows the load–displacement curves corresponding to this case. For Type I, the bending state is obtained after two transitions in Case I, which is concluded from the trend of load–displacement curves and the transition process shown in Fig. 15(d). For Type II, the transition similar to Case III is finished first, and then a transition like Case I is followed, as shown in Fig. 15(d).

Geometry of beam

Parameters	Value (mm)
R	28
H	8
S	12
W	8
t	1.25

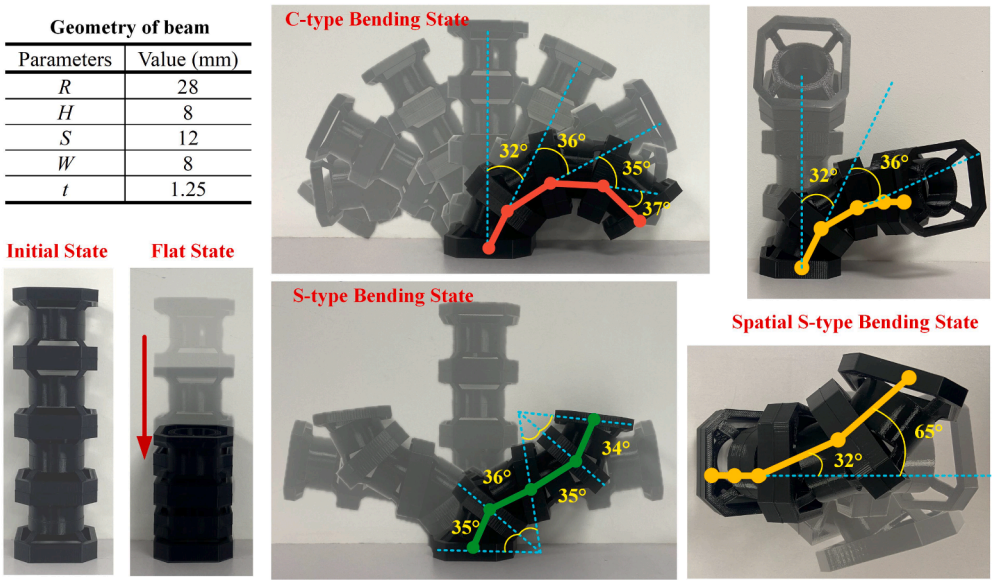

(a)

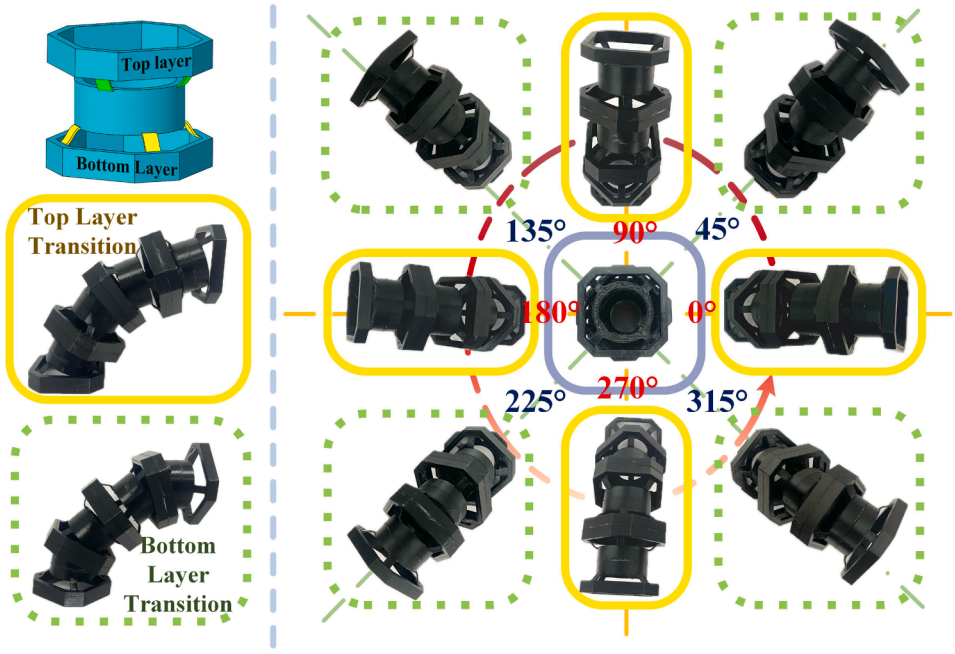

(b)

Fig. 17. Two types of multi-stable meta-structure.

2. Bending state to other bending state

If the current state is a bending state, an additional lateral load will introduce more feasible transitions. Here, several cases where the load is applied to different positions will be discussed. As shown in Fig. 16(a) and (b), a load is applied to the upward side of the octagon frame on the top layer, and two transitions similar to the situation in Fig. 11 are completed to reach the flat state. If the load is applied to the inclined side of the octagon frame on the top layer, two transitions similar to the situation in Fig. 10 are triggered to change the orientation of the bending state.

For Type II, the transitions become more complicated than those in Type I. As shown in Fig. 16(d), three loading positions will lead to three different cases. For Position I, the load is applied to the inclined side of the frame with a lower height. At this moment, only one transition occurs in the top layer, as shown in Fig. 16(c) and (d). For Position II, the load is applied to the inclined side with a higher height, resulting in two transitions from the inclined state to another inclined state. In the last case, when the load is applied to the upward side of the frame, a transition with three steps appears, as illustrated in Fig. 16(e) and (f). The bottom layer transits to a new inclined state first, and then two continuous transitions happen in the top layer. From the load–displacement response, it is easy to see that the three transitions all belong to the situation shown in Fig. 10.

The above results indicate that transitions of the double-layer unit are regarded as the combination of corresponding responses of two individual single layers. According to the configuration of the double-layer unit and the loading positions, plentiful bending orientations can be obtained.

5.3. Multi-layer structure

After understanding the mechanical properties of the single layer and double-layer units, a multi-layer structure with four double-layer Type I units stacking along the transverse direction is constructed, as shown in Fig. 17(a). The parameters of the beam are selected to reduce the size of the structure, as shown in Fig. 17(a). The capability of deformation is enhanced by the arrangement and combination of stable states in every single layer. The vertical lengthening and shortening are easy to obtain by axial loading and unloading. If layers transit to their inclined state in the same orientation step by step, a C-type bending state is obtained. For this eight-layer structure, the largest bending angle is able to reach 140° through the accumulation of the maximum inclined states with all layers. If the orientation of inclined states is different, a planar S-type bending state or a spatial S-type bending state could be formed.

Another multi-layer structure was fabricated with the Type II double-layer units, as illustrated in Fig. 17(b). As discussed before, two bending orientations could be realized in this double-layer unit. If all the top layers shown in Fig. 17(b) transit to their inclined states, a bending state is obtained, and another bending state is obtained when these transitions of all the bottom layers happen. In the top view, these two bending states exhibit different orientations, as shown in Fig. 17(b). Therefore, based on the Type II unit, the bending states of the multi-stable structure have eight orientations. Though the proposed multi-stable structure has the flexibility of deformation with multi-degree freedom, the actuating method will be considered in the future.

6. Conclusions

In this work, a family of multi-layer multi-stable metastructures has been proposed, designed, and investigated. Firstly, a single layer of this metastructure is designed and fabricated, for which the transitions between its different states are studied by both finite element methods and experiments. Specifically, two hourglass units, each comprising two layers, are devised as the fundamental building units to construct the multi-layer structure. The continuous transitions occurring in two or three steps are measured experimentally. Some conclusions can be summarized as follows:

1. A single layer comprising four preshaped beams exhibits five stable states, including one flat state and four inclined states. It is observed that the transitions from the initial state to the inclined state, induced by lateral compression, require lower loading and consume less energy than transitions from the initial state to the flat state under axial compression.
2. If a certain inclined state is designated as the final state, it is crucial to position the loading point within a corresponding range on the frame. When the loading position approaches the beam, there is a gradual decrease in the maximum load, while the required energy is increased. The transitions between inclined states are facilitated by lateral compression, and it is worth noting that an inclined state also can transit to the flat state if the load is applied to the mid-point of the frame arc between two upward beams.
3. Parametric analysis reveals that the stability of the inclined state is highly sensitive to the parameters, such as apex height, span, and thickness of the beam. Additionally, the radius of the circular frame becomes crucial, particularly when the beam width is relatively wide. To achieve a robust inclined stable state, it is recommended to maintain the value of H/t within the range of 6.5 to 20, while the value of S/H should ideally be lower than 1.75.
4. The load–displacement responses of the double-layer unit could be regarded as the combination and arrangement of responses of the single layer. Moreover, one or two bending orientations could be realized in one two-layer unit by the arrangement of beams.
5. Two examples of a multi-stable structure consisting of four double-layer units are constructed as an example to demonstrate its robust deformation capabilities, such as stretching, planar bending, and specialized bending. Through proper unit arrangement and design, the proposed multi-stable structures with multi-directional deformation capabilities offer new solutions for designing deployable structures or soft robotics.

CRediT authorship contribution statement

Shuangfeng Tan: Validation, Investigation, Formal analysis. **Diankun Pan:** Writing – original draft, Methodology, Funding acquisition, Formal analysis, Conceptualization. **Zhangming Wu:** Writing – review & editing, Visualization, Supervision.

Declaration of competing interest

The authors declare that they have no known competing financial interests or personal relationships that could have appeared to influence the work reported in this paper.

Data availability

The data that has been used is confidential.

Acknowledgement

This work was supported by the National Natural Science Foundation of China [grant No. 12202215], and China Postdoctoral Science Foundation [grant No. 2020M681805].

References

[1] K. Bertoldi, V. Vitelli, J. Christensen, M. van Hecke, Flexible Mechanical Metamaterials, Nature Reviews Materials 2 (2017) 17066.
[2] R. Khajehtourian, D.M. Kochmann, Soft adaptive mechanical metamaterials, Frontiers in Robotics and AI 8 (2021) 673478.
[3] C.P. de Jonge, H.M.A. Kolken, A.A. Zadpoor, Non-Auxetic Mechanical Metamaterials, Materials. 12 (4) (2019) 635.
[4] X. Wu, Y. Su, J. Shi, Perspective of additive manufacturing for metamaterials development, Smart Mater. Struct. 28 (2019) 093001.
[5] X. Tan, B. Wang, S. Zhu, S. Chen, K. Yao, P. Xu, et al., Novel multidirectional negative stiffness mechanical metamaterials, Smart Mater. Struct. 29 (2019) 015037.
[6] C. Ren, D. Yang, H. Qin, Mechanical performance of multidirectional buckling-based negative stiffness metamaterials: an analytical and Numerical study, Materials. 11 (7) (2018) 1078.
[7] J. Hua, H. Lei, Z. Zhang, C. Gao, D. Fang, Multistable cylindrical mechanical metastructures: theoretical and Experimental studies, J. Appl. Mech. 86 (2019) 071007.
[8] H. Fan, L. Yang, Y. Tian, Z. Wang, Design of metastructures with quasi-zero dynamic stiffness for vibration isolation, Compos. Struct. 243 (2020) 112244.
[9] V. Gupta, S. Adhikari, B. Bhattacharya, Exploring the dynamics of hourglass shaped lattice metastructures, Sci. Rep. 10 (2020) 20943.
[10] F.S.L. Bobbert, S. Janbaz, T. van Manen, Y. Li, A.A. Zadpoor, Russian doll deployable meta-implants: fusion of kirigami, origami, and multi-stability, Mater. Des. 191 (2020) 108624.
[11] R. Tao, L. Xi, W. Wu, Y. Li, B. Liao, L. Liu, et al., 4D printed multi-stable metamaterials with mechanically tunable performance, Compos. Struct. 252 (2020) 112663.
[12] Y. Cao, M. Derakhshani, Y. Fang, G. Huang, C. Cao, Bistable structures for advanced functional systems, Adv. Funct. Mater. 31 (2021) 2106231.
[13] D. Tan, J. Zhou, K. Wang, X. Zhao, Q. Wang, D. Xu, Bow-type bistable triboelectric nanogenerator for harvesting energy from low-frequency vibration, Nano Energy 92 (2022) 106746.
[14] T.-H. Ngo, I.T. Chi, M.-Q. Chau, D.-A. Wang, An energy Harvester based on a bistable origami mechanism, Int. J. Precis. Eng. Manuf. 23 (2022) 213–226.
[15] Y. Chi, Y. Li, Y. Zhao, Y. Hong, Y. Tang, J. Yin, Bistable and multistable actuators for soft robots: structures, materials, and functionalities, Adv. Mater. 34 (2022) 2110384.
[16] Y. Tang, Y. Chi, J. Sun, T.-H. Huang, O.H. Maghsoudi, A. Spence, et al., Leveraging elastic instabilities for amplified performance: spine-inspired high-speed and high-force soft robots. science, Advances 6 (eaaz6912) (2020).
[17] H. Yang, L. Ma, 1D and 2D snapping mechanical metamaterials with cylindrical topology, Int. J. Solids Struct. 204–205 (2020) 220–232.
[18] Y. Zhang, M. Tichem, F. van Keulen, A novel design of multi-stable metastructures for energy dissipation, Mater. Des. 212 (2021) 110234.
[19] R. Ahmad, A. Abdolhamid, P. Damiano, Snapping mechanical metamaterials under tension, Adv. Mater. 27 (2015) 5931–5935.

[20] A. Rafsanjani, D. Pasini, Bistable auxetic mechanical metamaterials inspired by ancient geometric motifs, Extreme Mech. Lett. 9 (2016) 291–296.
[21] K. Liu, T. Tachi, G.H. Paulino, Invariant and smooth limit of discrete geometry folded from bistable origami leading to multistable metasurfaces, Nat. Commun. 10 (2019) 4238.
[22] J.L. Silverberg, A.A. Evans, L. McLeod, R.C. Hayward, T. Hull, C.D. Santangelo, et al., Using origami design principles to fold reprogrammable mechanical metamaterials, Science 345 (2014) 647–650.
[23] S.A. Emam, D.J. Inman, A review on bistable composite laminates for morphing and energy harvesting, Appl. Mech. Rev. 67 (2015) 060803.
[24] B. Danish, P.M. Anilkumar, B.N. Rao, Suppression of cross-well vibrations of a bistable square cross-ply laminate using an additional composite strip, International Journal of Dynamics and Control. 11 (2023) 2680–2690.
[25] B. Haghpanah, L. Salari-Sharif, P. Pourrajab, J. Hopkins, L. Valdevit, Multistable shape-reconfigurable architected materials, Adv. Mater. 28 (2016), 07915-7920.
[26] F.S.L. Bobbert, S. Janbaz, A.A. Zadpoor, Towards deployable meta-implants, J. Mater. Chem. B 6 (2018) 3449–3455.
[27] F. Pan, Y. Li, Z. Li, J. Yang, B. Liu, Y. Chen, 3D pixel mechanical metamaterials, Adv. Mater. 31 (2019) 1900548.
[28] J. Qiu, J.H. Lang, A.H. Slocum, A curved-beam bistable mechanism, J. Microelectromech. Syst. 13 (2004) 137–146.
[29] J.-H. Jeon, T.-H. Cheng, I.-K. Oh, Snap-through dynamics of buckled IPMC actuator, Sens. Actuators, A 158 (2010) 300–305.
[30] Y. Huang, J. Zhao, S. Liu, Design optimization of segment-reinforced bistable mechanisms exhibiting adjustable snapping behavior, Sens. Actuators, A 252 (2016) 7–15.
[31] J. Hua, H. Lei, C.-F. Gao, X. Guo, D. Fang, Parameters analysis and optimization of a typical multistable mechanical metamaterial, Extreme Mech. Lett. 35 (2020) 100640.
[32] H. Yang, L. Ma, Multi-stable mechanical metamaterials by elastic buckling instability, J. Mater. Sci. 54 (2019) 3509–3526.
[33] B. Chen, L. Chen, B. Du, H. Liu, W. Li, D. Fang, Novel multifunctional negative stiffness mechanical metamaterial structure: tailored functions of multi-stable and compressive mono-stable, Compos. B Eng. 204 (2021) 108501.
[34] T.R. Giri, R. Mailen, Controlled snapping sequence and energy absorption in multistable mechanical metamaterial cylinders, Int. J. Mech. Sci. 204 (2021) 106541.
[35] H. Fang, K.W. Wang, S. Li, Asymmetric energy barrier and mechanical diode effect from folding multi-stable stacked-origami, Extreme Mech. Lett. 17 (2017) 7–15.
[36] B. Haghpanah, L. Salari-Sharif, P. Pourrajab, J. Hopkins, L. Valdevit, Multistable shape-reconfigurable architected materials, Adv. Mater. 28 (2016) 7915–7920.
[37] L.-C. Wang, W.-L. Song, H. Fang, D. Fang, Reconfigurable force–displacement profiles of the square-twist origami, Int. J. Solids Struct. 241 (2022) 111471.
[38] A.L. Wickeler, S. Asm, H.E. Naguib, Triangular-based origami: modelling and testing the parameterized design for geometrical and mechanical analysis, Thin-Walled Struct. 173 (2022), 108993.
[39] F. Mattioni, P. Weaver, K. Potter, M. Friswell, Analysis of thermally induced multistable composites, Int. J. Solids Struct. 45 (2008) 657–675.
[40] I.K. Kuder, A.F. Arrieta, P. Ermanni, Design space of embeddable variable stiffness bi-stable elements for morphing applications, Compos. Struct. 122 (2015) 445–455.
[41] S. Mostafavi, M. Golzar, A. Alibeigloo, On the thermally induced multistability of connected curved composite plates, Compos. Struct. 139 (2016) 210–219.
[42] V. Chillara, M. Dapino, Mechanically-prestressed bistable composite laminates with weakly coupled equilibrium shapes, Compos. B Eng. 111 (2017) 251–260.
[43] W. Jiang, M. Li, Y. Yao, F. Dai, Design of a multistable composite laminate by variable cross-section method and applying the displacement constraint, Mater. Des. 147 (2018) 35–47.
[44] Z. Zhang, H. Wu, X. He, H. Wu, Y. Bao, G. Chai, The bistable behaviors of carbon-fiber/epoxy anti-symmetric composite shells, Compos. B Eng. 47 (2013) 190–199.
[45] H. Lee, J.-G. Lee, J. Ryu, M. Cho, Twisted shape bi-stable structure of asymmetrically laminated CFRP composites, Compos. B Eng. 108 (2017) 345–353.
[46] C.G. Diaconu, P.M. Weaver, F. Mattioni, Concepts for morphing airfoil sections using bi-stable laminated composite structures, Thin-Walled Struct. 46 (2008) 689–701.
[47] I.K. Kuder, A.F. Arrieta, W.E. Raither, P. Ermanni, Variable stiffness material and structural concepts for morphing applications, Prog. Aerosp. Sci. 63 (2013) 33–55.
[48] O. Bilgen, A.F. Arrieta, M.I. Friswell, P. Hagedorn, Dynamic control of a bistable wing under aerodynamic loading, Smart Mater. Struct. 22 (2013) 025020.
[49] Y. Zhang, M. Tichem, K. Fv, Rotational snap-through behavior of multi-stable beam-type metastructures, Int. J. Mech. Sci. 193 (2021) 106172.
[50] Y. Zhang, Q. Wang, M. Tichem, F. van Keulen, Design and characterization of multi-stable mechanical metastructures with level and tilted stable configurations, Extreme Mech. Lett. 34 (2019) 100593.
[51] S. Park, D. Hah, Pre-shaped buckled-beam actuators: theory and experiments, Sens. Actuators, A 148 (2008) 186–192.
[52] M. Alturki, R. Burgueño, Response characterization of multistable shallow domes with cosine-curved profile, Thin-Walled Struct. 140 (2019) 74–84.
[53] H. Hussein, M.I. Younis, Analytical study of the snap-through and bistability of beams with arbitrarily initial shape, J. Mech. Robot. 12 (4) (2020) 4045844.